Preparation and Characterization of Polyurethane Porous Membranes by Particulate-leaching Method

Salvatore Iannace, Ernesto Di Maio and Luigi Nicolais

Institute of Composite Materials Technology (ITMC-CNR) &
Department of Materials and Production Engineering,
University of Naples, Piazzale Tecchio 80, 80125 Naples-Italy

Received: 27th April 2001; Accepted: 26th June 2001

SUMMARY

Highly porous polyurethane foams were prepared by the particulate-leaching technique, using NaCl as water-soluble solid phase. Melt compounding and compression moulding were used to prepare polymer/salt composite samples. Foams with controlled porosity, surface/volume ratio and pore dimension distribution were therefore obtained after dissolution of salt in distilled water. Dissolution kinetic was evaluated and modelled as a function of filler composition and its size distribution. Kinetic increased by rising salt concentration and by reducing its average size.

Mechanical properties of the foams were correlated to their morphological structure and to the properties of polymeric component.

INTRODUCTION

Recently, in many fields of material science and medicine a new philosophy based on biomimetic concepts is employed to optimize structure and properties of materials. In particular, the possibility of imitating nature in the design and preparation of natural tissue substitutes in biomedical field can be useful for two reasons. It can be used either to reproduce the morphological architecture and the biomechanical functionality of the substituted tissue or to provide a permanent or temporary scaffold for the regeneration of natural tissues. In orthopaedics, bone substitutes should therefore present a cellular structure, with open cells and cell dimension ranging between 100 and 200μm, in order to provide a substrate for the body's natural ability to repair injured bone with new bone tissue. However, fracture healing results from the formation of new bone that can then remodel itself to optimize its mechanical function for its particular skeletal location[1,2]. The initial biomaterial should provide temporary mechanical strength to the reconstructed region and should allow or induce the region to reconstitute itself with new bone[3-7].

Much in literature has been done about foams and cellular solids. Mechanical and thermal properties have been investigated and have been related to morphology and structure of the cells. Recently a new technique to produce these structures has been proposed. Open cell, highly porous solids can be produced by a particulate-leaching process[6-12]. These highly porous polymer membranes can be used as scaffold for cell seeding and growth in the biomedical field and tissue engineering. Tissue ingrowth is usually affected by physical and chemical characteristics of the polymer as well as the cellular structure determined by its porosity, surface/volume ratio, interconnected pore structure.

This technique often involves the dissolution of a water-soluble solute (sugar, salt) from a polymer/solute composite system. The overall process involves complex mechanisms of solvent penetration into the polymeric matrix, dissolution of the solid phase and diffusion through the interconnected pores left by the dispersed phase. The final morphology, which determines physical and mechanical properties of the foam, is therefore strictly correlated to the initial composition of the composite and to the size distribution of the solute particles. Moreover, it can be modulated by a proper choice of the matrix component and by the techniques employed for the preparation of the composite. For example, in most of the works reported in literature[8-12], thin composite membranes were prepared by solvent casting procedures on polymer/solute/solvent systems. It has been showed that the porosity obtained by using this technique is usually higher than that theoretically expected, due to pores created during solvent evaporation. Organic solvent residues can remain in the sponges and may be harmful to adherent cells, protein growth factors or nearby tissues. That is why macroporous sponges from synthetic biodegradable polymers are fabricated also by using high-pressure carbon dioxide[5].

In this work, which is part of a wider research project on bone substitute[13], composites were prepared by using polyurethane as polymeric matrix and NaCl as solute. Conventional polymer process technologies such as melt compounding and compression moulding were used for the preparation of samples. Dissolution kinetic was evaluated with the aim of clarifying the effect of initial composition and salt size distribution. Moreover, physical and mechanical properties were investigated in order to correlate structure, morphology and properties of the foams.

EXPERIMENTAL

Materials

Polyurethane used was Corethane (BIONATE 55D, PTG). Sodium chloride (Aldrich) was ground with a mechanical mill to obtain a fine particulate. The ground particles were sieved with USA Standard Testing Sieves (ASTM 11 Specification) with opening of 106 μm (No 140), 150 μm (No 100) and 212 μm (No 70) placed on a sieve shaker (model IG/3-EXP).

Processing method

Polyurethane cellular structures were prepared by a particulate-leaching technique that consisted of the following steps.

1) Salt particles were ground and sieved.
2) Sieved particles were added to polyurethane and mixed at 200°C for 1 min at 150 rpm (Haake). Four different polymer-salt compositions were used in our studies: 70%wt salt; 80%wt salt; 85%wt salt; 90%wt salt. For each composition, sieved salt particles of two different sizes (d) were employed: $0<d<150$ μm (distribution A) and $106<d<212$ μm (distribution B), as summarised in Table 1.
3) The resulting PU/salt composite was moulded into proper shape by compression moulding.
4) The samples were immersed in distilled water on a magnetic stirrer at 100 rpm, 25 °C (the water was changed every 12 h) to leach out the salt.
5) The weight of the samples was evaluated to study the dissolution-absorption kinetic.
6) The salt-free PU samples were vacuum dried for 48 h.

Mechanical properties

Tensile and compressive tests were carried out on an Instron testing machine (model 4204) with a 5 kN load cell. Tensile tests were performed on dog bone samples, according to ASTM D638 specification. The crosshead speed was 5 mm/min. Compressive tests were performed on cylindrical samples (thickness=10 mm, diameter=10 mm), with a crosshead speed of 2.54 mm/min.

Scanning electron microscopy (SEM)

The samples were sectioned in liquid nitrogen and coated with gold using a sputter coater (Emscope SC500). The morphology of the fracture surface was studied by using a LEICA mod. S440 scanning electron microscope operating at 20 kV.

Table 1 Composition of the materials tested, symbols utilized in the dissolution kinetic evaluation and morphology parameters of the cellular structures tested

Composition	Pore dimension d (μm)	Symbol	Porosity p	Tortuosity T
70 wt% NaCl-30 wt% PU	d<150	Δ 70A	0.538	455
80 wt% NaCl-20 wt% PU	d<150	■ 80A	0.666	334
85 wt% NaCl-15 wt% PU	d<150	○ 85A	0.739	73.3
90 wt% NaCl-10 wt% PU	d<150	◆ 90A	0.818	17.4
70 wt% NaCl-30 wt% PU	106<d<212	▲ 70B	0.538	4841
80 wt% NaCl-20 wt% PU	106<d<212	❑ 80B	0.666	1357
85 wt% NaCl-15 wt% PU	106<d<212	● 85B	0.739	281
90 wt% NaCl-10 Wt% PU	106<d<212	◊ 90B	0.818	147

RESULTS AND DISCUSSION

Release kinetics

Figures 1-2 show the time evolution of the weight of the samples during the salt dissolution process. In Figure 1 weight loss of the samples containing salt with size distribution A (70 A-90 A) is reported versus square root of time. In Figure 2 the weight loss of the two salt distributions are compared (70 A, 70 B, 85 A, 85 B). As expected, an increase of salt concentration speeds up the salt release process, and this phenomenon was observed in similar composite systems[14-18]. The effect of particle size is also relevant (Figure 2), and the complex mechanism involved during the salt dissolution process will be discussed below.

The quantitative treatment of mechanisms involved during solute dissolution and diffusion has been extensively analyzed in systems utilized for drug release purposes. The simplest assumption in these models is that the dissolution of the solid phase incorporated in the polymeric matrix is instantaneous and the rate of the drug release is controlled by the rate of diffusion of the dissolved drug and its solubility within the matrix. In this model, the interface between the bathing solution and the solid drug moves towards the interior. The movement of the salt/water solution boundary, in principle, is also affected by surface tension of polymer and water. The model should therefore take into account this aspect; however, in our case, as the polymer is wettable, the exchange kinetics of salt and water is likely not to be controlled by surface phenomena. Derivation of the mathematical model developed by Higuchi[19, 20], involves the following assumption[21, 22]: a) a pseudo-steady state during the release, b) the

Figure 1 Weight loss during salt dissolution process; all composition, distribution A

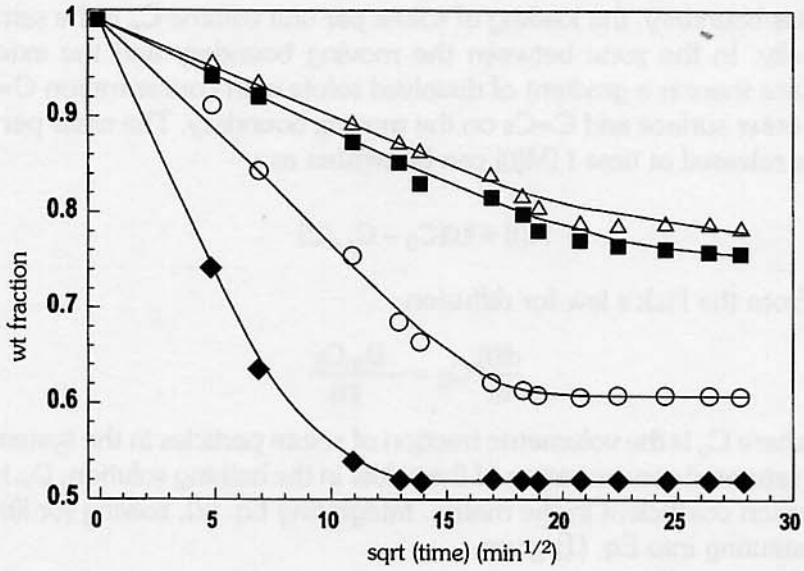

Figure 2 Comparison between dissolution kinetics for the two distributions, A and B

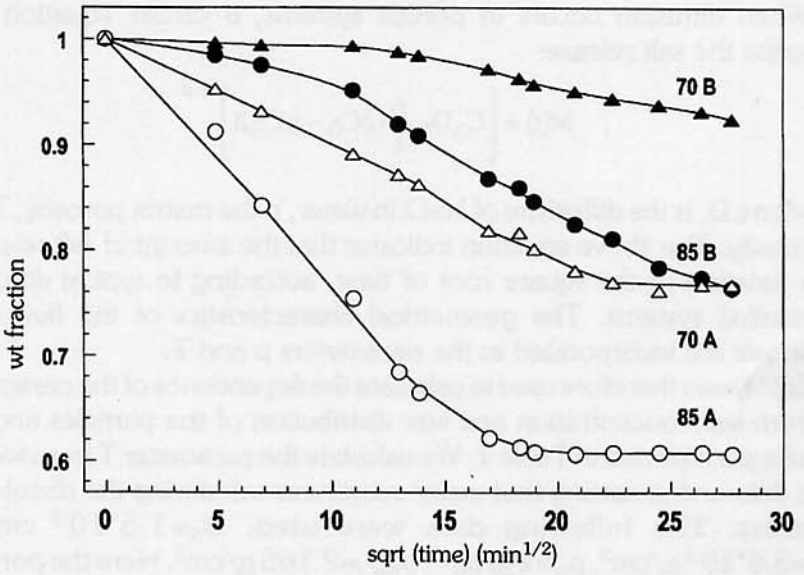

diameter of the particles is less than the average distance of drug diffusion through the matrix, c) the bathing solution provides sink conditions at all times, d) the diffusion coefficient of drug in the matrix remains constant.

The Higuchi model involves a moving boundary located at distance l(t) from the external surface after extraction for a time t. In the zone ahead of this boundary, the loading of solute per unit volume C_0 is the same as initially. In the zone between the moving boundary and the external surface there is a gradient of dissolved solute with concentration C=0 at the outer surface and C=Cs on the moving boundary. The mass per unit area released at time t (M(t)) can be written as :

$$M(t) = l(t)[C_0 - C_s / 2] \tag{1}$$

From the Fick's law for diffusion:

$$\frac{dl(t)}{dt} C_0 = -\frac{D_m C_S}{l(t)} \tag{2}$$

where C_0 is the volumetric fraction of solute particles in the system, C_s the saturated concentration of the solute in the bathing solution, D_m is the diffusion coefficient in the matrix. Integrating Eq. (2), solving for l(t) and substituting into Eq. (1) gives:

$$M(t) = [C_S D_m (2C_0 - C_S)t]^{1/2} \tag{3}$$

When diffusion occurs in porous systems, a similar equation can describe the salt release:

$$M(t) = \left[C_S D_S \frac{p}{T} (2C_0 - pC_S)t \right]^{1/2} \tag{4}$$

where D_s is the diffusivity of NaCl in water, p the matrix porosity, T the tortuosity. The above equation indicates that the amount of salt released is a function of the square root of time, according to typical diffusion controlled systems. The geometrical characteristics of the fluid-filled channels are incorporated in the parameters p and T.

Eq. (4) was therefore used to calculate the dependence of the parameter T from salt concentration and size distribution of the particles and the results are reported in Table 1. We calculate the parameter T from weight loss data and assuming that water substitutes salt during the dissolution process. The following data were used: $D_S=1.5*10^{-5}$ cm^2/s, $C_S=3.6*10^{-1}$ g/cm^3, $\rho_w=1$ g/cm^3, $\rho_{NaCl}=2.165$ g/cm^3. Here the porosity was assumed to be equal to the volumetric fraction of the salt in the system. This assumption is based on the following points: i) the volumetric fraction of the salt is above the percolation threshold so that all the salt is removed from the system; ii) the composites were not prepared by casting

procedures so that additive pores, usually created by the evaporation of a solvent during the sample preparation[8], should not be present.

The linear behaviour observed in the initial part of the curves of Figure 1 confirms that, at least in the initial stage of the leaching process, the diffusion-controlled mechanism can be considered valid. As expected, an increase of salt concentration speeds up the release kinetic and this is correlated to both an increase of porosity p and a decrease of tortuosity T (Table 1).

Composites prepared with salt particles of smaller dimensions (distribution A, d<150 mm) show faster release (Figure 2) and the parameter T, calculated from experimental data, is lower in this case (Table 1).

The tortuosity factor, defined in Eq. (4), takes into account the effective path length in the pores. In homogeneous, isotropic porous media this factor equals 3, but in pores of varying cross-section (varying radii) diffusion may result in abnormally large values[23-24]. In a recent paper three mechanisms that could be responsible of retardation of diffusional release of macromolecular drugs from porous hydrophobic polymer matrices were investigated[17]. The "presence of constricted pore geometry" was considered to be the primary explanation of this retardation, compared to the other two mechanism related to "concentration-dependent diffusion" and "random pore topology". However, in the case of salt release, due to the saturation of the solute in the pores, the dissolution rate can become the rate-determining step, which results in a dramatic reduction of the release kinetic and, as consequence, in high tortuosity factors.

The simple Eq. (4) was used to explain the effect of initial concentration of salt and pore structure assuming weight loss controlled by diffusion of the solute in the pores. However, the situation is more complex since another process occurred in our case during the leaching of the salt. The polymer employed as matrix is an elastomeric polyurethane and its elastic modulus is quite low (45.5 MPa in tensile test). During salt dissolution, an osmotic pressure can develop inside the pores, due to the high salt concentration. This pressure can work against the cell walls leading to an increase of the pore dimensions and, as consequence, to an increase of the amount of water absorbed inside the pores. This effect usually occurs when the solute is separated from the solvent by a membrane that is impermeable to the solute. In principle, higher swelling in our polyurethane/ salt system, can be obtained if resistance to salt diffusion is increased through morphological restrictions. This is possible by modifying the pore morphology through the control of salt concentration and size distribution.

The "Fickian" behaviour, observed in materials A, was analyzed according to Eq. (4). However the final weight reached by the composites does not equal the theoretical values and this is due to the deformation of the matrix, caused by the osmotic pressure, which results in higher amount of water driven in the pores.

For samples B this process is more evident. The linear plateau reached by the samples is very far from the theoretical values and most of the materials B (from 70% to 85% of salt) showed a linear relationship in the weight loss-time curve (Figure 3), suggesting that a mechanism different than Fickian is occurring in this case. The very high tortuosity coupled with the high swelling of the matrix, observed in samples B (70 B, 80 B), suggests that the rate determining step is not the diffusion of salt in the pores, but it could be related to salt dissolution process and/or swelling of the polymeric matrix.

With the hypothesis of "Fickian" behaviour for all the samples A, the weight loss data were used to calculate the kinetic of salt release and to calculate the effective diffusion coefficient $D_e = D_s\, p/T$ from Eq. (4). In Figure 4 is reported the D_e versus porosity p. Experimental data were fitted by using the following equation, that describes the dependence of the diffusivity in percolating systems[25].

$$D_e \propto (p - p_c)^{\mu} \tag{5}$$

where D_e is the effective diffusivity, p is the porosity of the system, p_c is the critical porosity above which an infinite (sample spanning) pore spans the network and μ is the transport exponent (independent of the microscopic details of the system). By using a percolation threshold p_c equal to 0.6, as suggested by Caraballo et al.[26], the exponent μ is equal to 2.2, very close to the value reported by Sahimi (25) (μ =2.0). The value was obtained from the fitting of the effective diffusivity of samples whose porosity was above the percolation threshold (80 A, 85 A and 90 A).

Morphology and mechanical properties

The different cellular morphologies obtained by modifying salt composition and size are shown in Figure 5a-b. The good dispersion of salt particles in the polymer melt during mixing operations results in a uniform cell morphology within the samples. The absence of the salt crystals in the micrographs suggests that the dissolution of the salt process was complete, as confirmed by the final weight of the foamed samples after drying. This means that pores are all interconnected and, by definition, the achieved structure is an open-cell one. In fact, the particular procedure used to

Figure 3 Dissolution kinetics for the distribution B

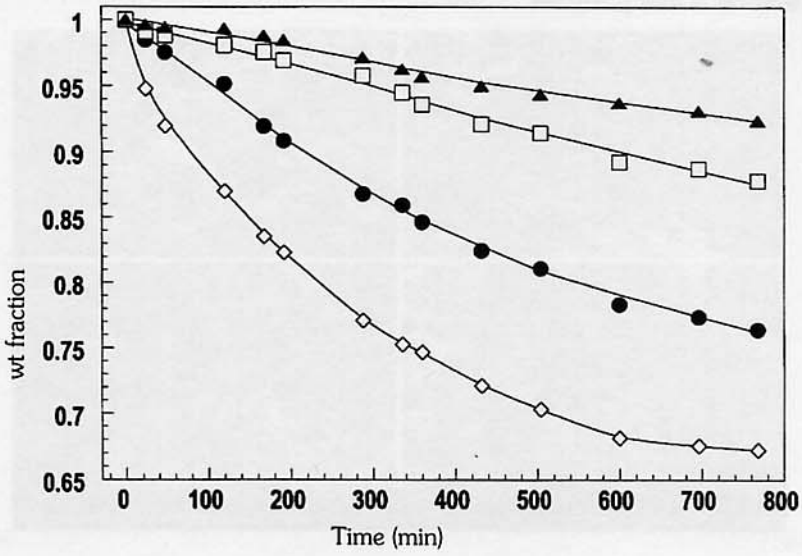

Figure 4 Equivalent diffusivity versus porosity for distribution A

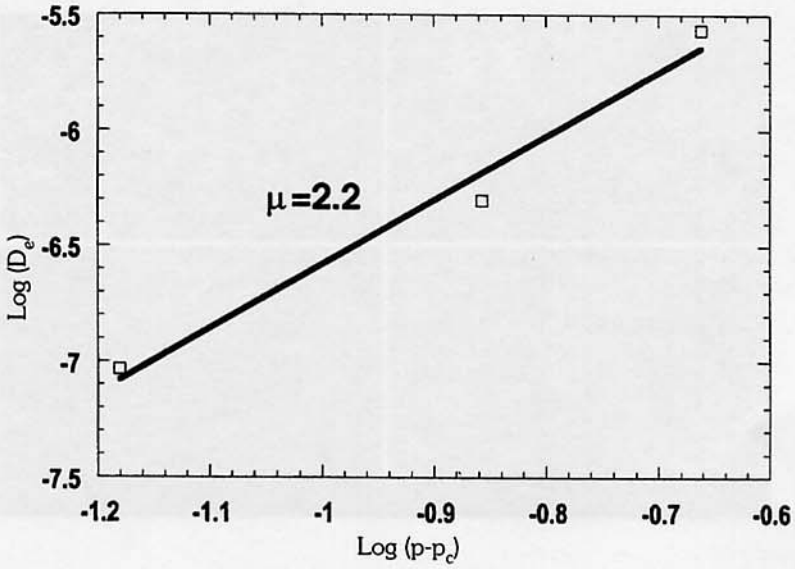

produce these foams gives a structure that is not properly open-cell and is more similar to a closed cell one (this will also be marked through the analysis of the mechanical properties). Inspection of the micrographs shows the presence of very small pores interconnecting the cells, created

Figure 5a SEM photomicrographs of cross sections of PU foams prepared with distribution A salt particles

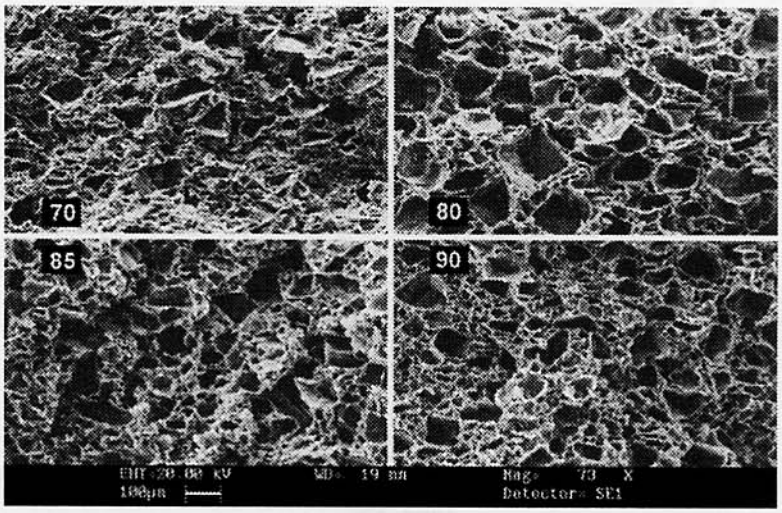

Figure 5b SEM photomicrographs of cross sections of PU foams prepared with distribution B salt particles

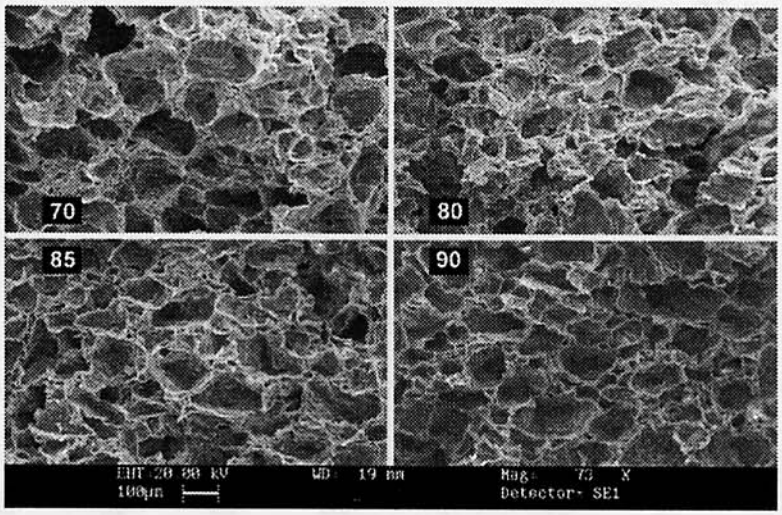

after the remotion of the touching salt crystals. The size of these pores is much smaller than that of main cells and for this reason the morphology detected by SEM recalls that of closed cell structures.

An increase of salt concentration leads to foams with a higher number of interconnected pores (Figure 5a) and this justifies the faster dissolution

kinetic observed when salt concentration was raised. Cellular morphology is greatly influenced by the size distribution of salt particles. Salt of narrower distribution (Type B) resulted in foams with a more uniform cell size, as shown in Figure 5b.

As discussed below, the different cellular morphology resulting from to the two sets of salt crystals size distributions employed, leaded to foams with equal density but with different mechanical properties, either in compression and in tensile tests, as reported in Tables 2-3. In order to correlate the mechanical properties of the foams to those of the polymeric matrix, tensile tests have been performed on pure PU. The material showed an elastic modulus of 45.5±5 MPa, a tensile strength of 49.3±2 MPa and a deformation at break of 7.3±0.3 mm/mm.

Compressive curves of samples A are reported in Figure 6. As expected, an increase of density results in foams of higher stiffness. Curves show the typical behaviour of elastomeric foams characterized by an initial linear portion, related to the elastic deformation of cells, a macroscopic yield and a densification part, identified by a progressive increase of the stress versus strain. This behaviour has been observed in both open and closed cell structures[27-29], even though the presence of cell walls determines stretching phenomena that influence the state of the stress in the material. In general, if the cell walls are much thinner than the cell edges, the deformation is governed by edge bending, while in cells of thicker walls, the cell wall stretching becomes the dominant behaviour. In the former case, the compressive curves are characterized by an horizontal plateau after the macroscopic yielding, while an increase of the stress is generally observed in the latter case, were the contribution of the cell stretching becomes significant. The presence of both bending and stretching has been modelled by Gibson and Ashby, the two authors combined linearly the two effects, leading to a general expression for the modulus of the foam as a function of the reduced density[29]:

$$\frac{E^*}{E^S} = C_1\left(\frac{\rho^*}{\rho^S}\right)^2 + C_2\frac{\rho^*}{\rho^s} \qquad (6)$$

where E is the Young's Modulus, ρ is the density, the superscript "s" indicates a property of the solid cell wall material while a superscripted asterisk "*" refers to a property of the foams itself. In this equation C_1, the contribution proportional to the square of the reduced density, is correlated to the bending mechanism. The other contribution C_2 is correlated to the stretching of the cell walls. The experimental data, reported in Table 2,

Table 2 Compressive test results

Sample	Density (g/cm^3)	Young's modulus E (MPa)	Yield stress (MPa)	Yield strain (mm/mm)
70A	0.461	11.1 ± 1.7	0.93 ± 0.05	0.086 ± 0.01
80A	0.333	6.13 ± 0.55	0.31 ± 0.03	0.051 ± 0.008
85A	0.261	5.52 ± 0.74	0.26 ± 0.05	0.050 ± 0.004
90A	0.182	1.5 ± 0.25	0.089 ± 0.01	0.064 ± 0.01
70B	0.461	6.11 ± 1.62	0.79 ± 0.06	0.15 ± 0.03
80B	0.333	4.52 ± 0.79	0.34 ± 0.02	0.88 ± 0.01
86B	0.261	3.82 ± 0.35	0.19 ± 0.01	0.054 ± 0.007
90B	0.182	1.98 ± 0.37	0.12 ± 0.01	0.065 ± 0.01

Table 3 Tensile test results

Sample	Density (g/cm^3)	Young's modulus E (MPa)	Stress at break (MPa)	Strain at break (mm/mm)
70A	0.461	9.5 ± 0.5	7.8 ± 0.48	2.5 ± 0.18
80A	0.333	5.06 ± 0.34	3.85 ± 0.39	1.73 ± 0.15
85A	0.261	4.37 ± 0.15	2.18 ± 0.26	1.27 ± 0.11
90A	0.182	3.19 ± 0.35	1.21 ± 0.31	0.85 ± 0.12
70B	0.461	5.41 ± 0.41	5.7 ± 0.62	2.15 ± 0.15
80B	0.333	4.58 ± 0.39	3.42 ± 0.27	1.59 ± 0.24
86B	0.261	3.39 ± 0.25	2.54 ± 0.34	1.44 ± 0.15
90B	0.182	2.69 ± 0.26	1.59 ± 0.23	1.35 ± 0.18

were fitted with Eq. (6); the constant C_1 and C_2 were used as independent parameters. The results are shown in Figure 7 and the constants for foams A were C_1=0.85 and C_2=0.15. The higher value of C_1, compared to C_2, suggests that, in foams A, the bending mechanism is predominant. A similar analysis was done on samples B and the results are reported in the same figure. In this case C_1=0, C_2=0.29 and the modulus grows linearly with the foam density, suggesting that the deformation is controlled by the stretching behaviour.

The different deformation mechanisms observed in the two sets of foams resulted in materials with different mechanical performances. Selected compressive curves of the two sets of samples are compared in Figure 8. This is the evidence that the dependence of the compressive properties with the density of these materials cannot be simply analyzed in presence of non-uniform cellular morphology and is still a crucial problem for developing suitable model for the prediction of the properties

Figure 6 Stress-strain curves in compressive tests for all composition, distribution A

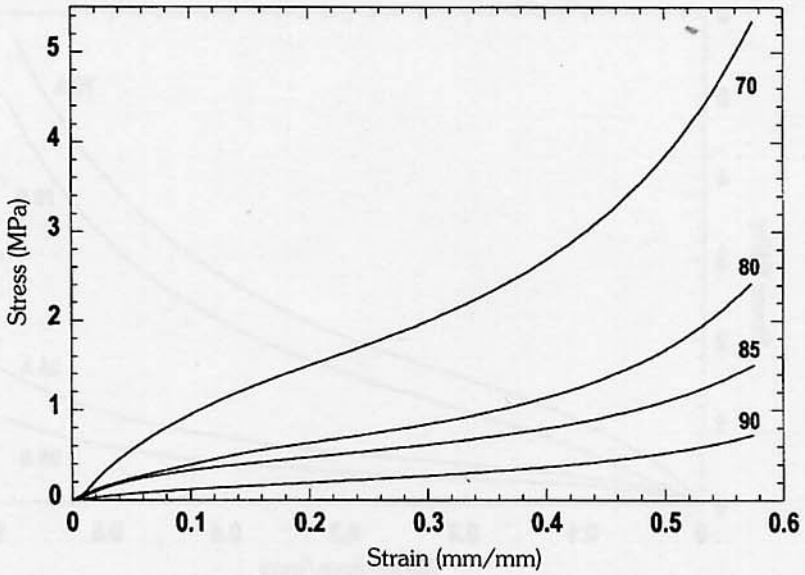

Figure 7 Young modulus versus volumetric polymer fraction in compressive tests. Open symbols - distribution A, solid symbols - distribution B

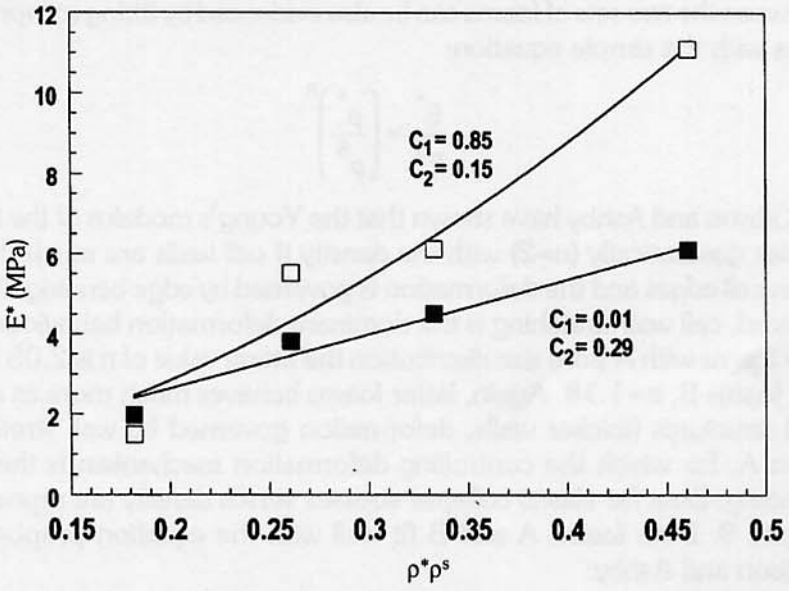

of cellular solids. At the local scale, other characteristics, such as the geometrical arrangement of the cell element, angles of intersection between edges, shape of the edges and of cell walls are of relevant

Figure 8 Stress-strain curves in compressive tests, comparison between the two distributions

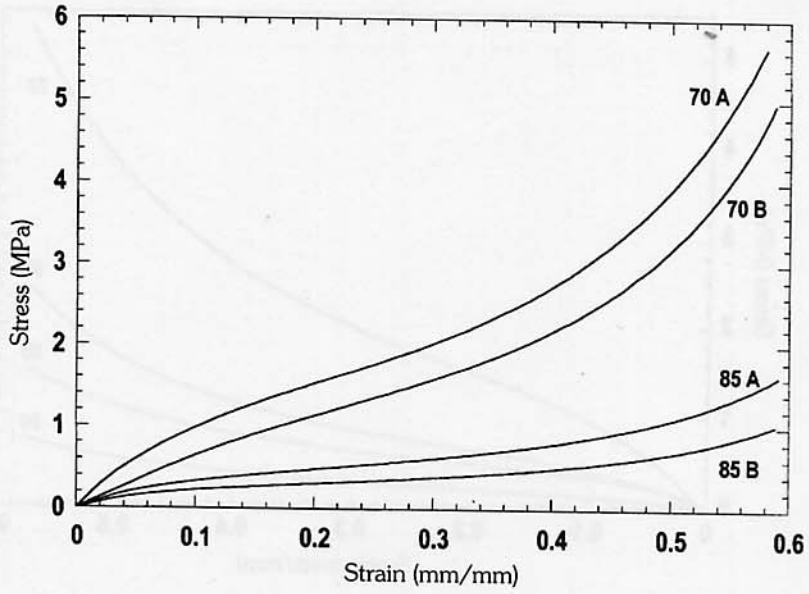

importance in the definition of the mechanical properties[30]. The difference between the two sets of foams can be also evidenced by fitting compressive data with the simple equation:

$$\frac{E^*}{E^S} = \left(\frac{\rho^*}{\rho^S}\right)^n \tag{7}$$

Gibson and Ashby have shown that the Young's modulus of the foams varies quadratically (n=2) with the density if cell walls are much thinner than cell edges and the deformation is governed by edge bending. If n=1, instead, cell wall stretching is the dominant deformation behaviour[29,30]. For foams with A pore size distribution the fitting value of n is 2.05 while, for foams B, n=1.18. Again, latter foams behaves much more as closed cell structures (thicker walls, deformation governed by wall stretching) than A, for which the controlling deformation mechanism is the edge bending. Data for elastic collapse stresses versus density are reported in Figure 9. Both foams A and B fit well with the equation proposed by Gibson and Ashby:

$$\frac{\sigma_{el}^*}{E^s} \approx 0.3\left(\frac{\rho^*}{\rho^S}\right)^2\left(1+\left(\frac{\rho^*}{\rho^S}\right)^{1/2}\right)^2 \tag{8}$$

Figure 9 Elastic collapse stresses versus volumetric polymer fraction in compressive tests. Open symbols - distribution A, solid symbols - distribution B

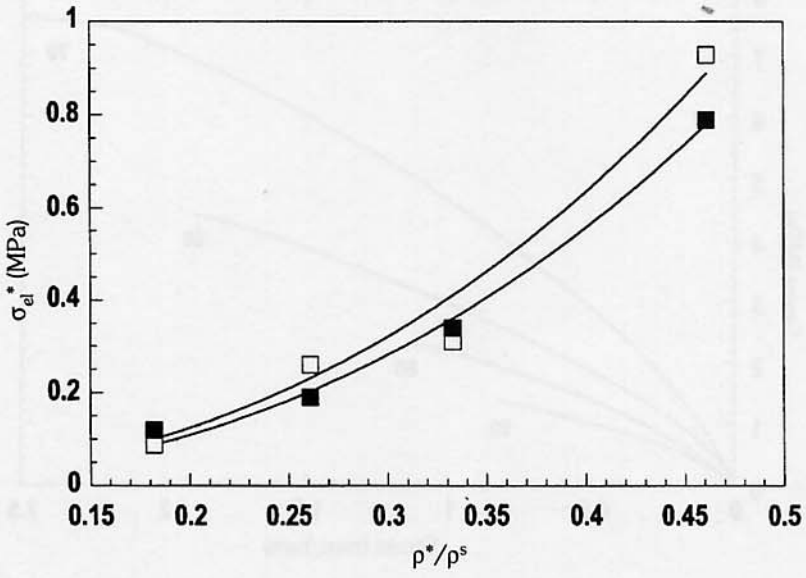

valid for both open and closed cell (in closed cells structures the gas entrapped into the cells is responsible for another contribution, gas pressurization, but in our foams air can easily flow away from the cells and cannot contribute to the compressive stiffness).

Tensile tests of samples A are reported in Figure 10. Again, like in compressive tests, the two distributions of pores are subjected to different deformation mechanism, as demonstrated by fitting tensile tests results with Eq. (6). The quadratic contribution is negligible for foams B while both the terms C_1 and C_2 contribute to the deformation of foams A, as reported in Figure 11.

CONCLUSION

Particulate-leaching method was used to prepare highly porous cellular solids. Polymer foams of definite porosity, surface/volume ratio, pore dimension and open cell morphology were obtained. The foam properties depend only on the initial salt weight fraction and particle size.

Mechanical tests have revealed the strong dependence of the properties of the cellular solids on the pore size distribution, both in compressive and in tensile tests. Not only the final properties but also the deformation mechanism is a function of the pore size distribution.

Figure 10 Stress-strain curves in tensile tests for all composition, distribution A

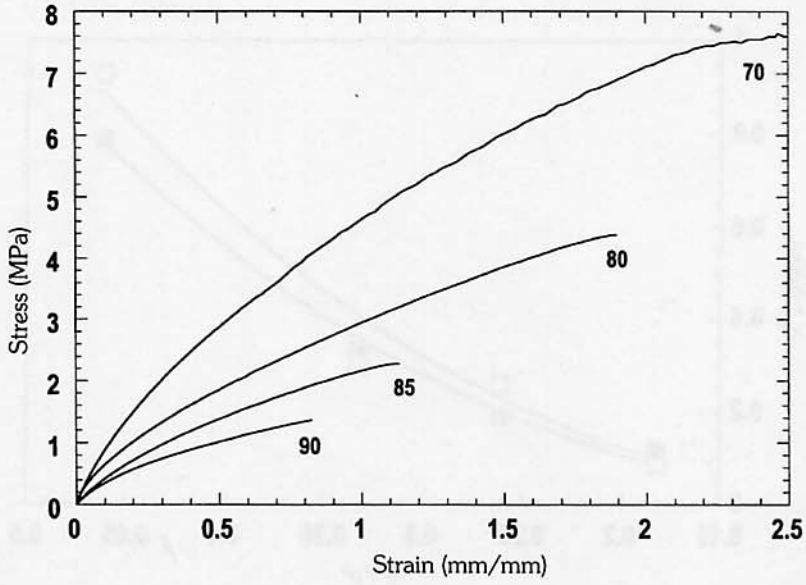

Figure 11 Young Modulus versus volumetric polymer fraction in tensile tests

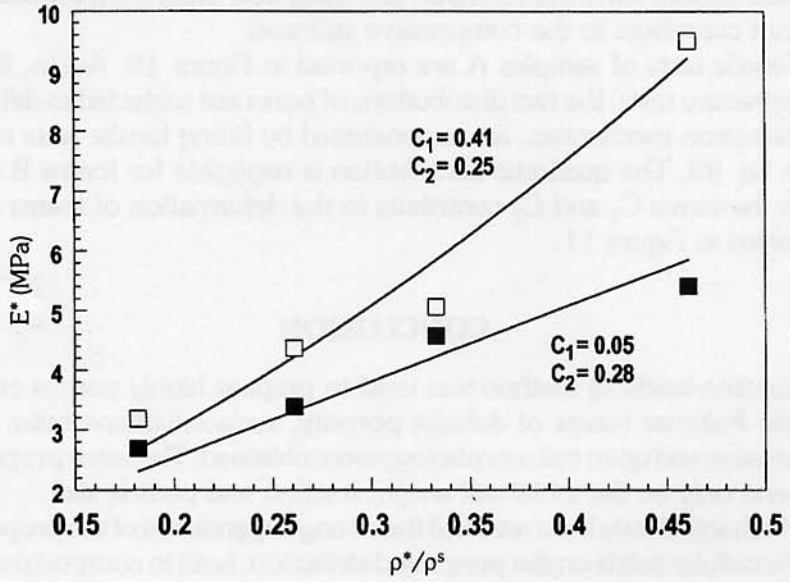

REFERENCES

1. Boyce S.T., in Human Biomaterials Applications, D.L. Wise et al., Humana Press Inc., Totowa, NJ, (1996), 347
2. Ambrosio L., Peluso G., Davis P.A., in Human Biomaterials Applications, D.L. Wise et al., Humana Press Inc., Totowa, NJ, (1996), 3
3. Yaszemski M.J., Payne R.G., Mikos A.G., Biomaterials, **17** (1996) 175
4. Fabbri M., Celotti G.C., Ravaglioli A., Biomaterials, **16** (1995) 225
5. Wald H.L., Sarakinos G., Lyman M.D., Mikos A.J., Vacanti J.P., Langer R., Biomaterials, **14** (1993) 270
6. Mooney D.J., Baldwin D.F., Suh N.P., Vacanti J.P., Langer R., Biomaterials, **17** (1996) 1417
7. Ishaug-Riley S.L., Crane-Kruger G.M., Yamszeski M.J., Mikos A.J., Biomaterials, **19** (1998) 1405
8. Mikos A.G., Thorsen A.J., Czerwonka L.A., Bao Y., Langer R., Winslow D.N., Vacanti J.P., Polymer, **35** (1994) 1068
9. Wald H.L., Sarakinos G., Lyman M.D., Mikos A.G., Vacanti J.P., Langer R., Biomaterials, **14** (1993) 270
10. de Groot J.H., de Vrijer R., Pennings A.J., Klompmaker J., Veth R.P.H., Jansen H.W.B., Biomaterials, **17** (1996) 163
11. Lo H., Ponticiello M.S., Leong K.W., Tissue Eng., **1** (1995) 15
12. Widmer M.S., Gupta P.K., Lu L., Meszlenyi R.K., Evans G.R.D., Brandt K., Savel T., Gurlek A., Patrick C.W. Jr, Mikos A.J., Biomaterials, **19** (1998) 1945
13. Biomimetic composites as bone substitute compounds, CNR-MFSTA II, 1998
14. Di Colo G., Biomaterials, **13** (1992) 850
15. Miller E.S., Peppas N.A., Winslow D.N., J. Membr. Sci., **14** (1983) 79
16. Siegel R.A., Kost J., Langer R., J. Controlled Release, **8** (1989) 223
17. Siegel R.A., Langer R., J. Controlled Release, **14** (1990) 153
18. Sheppard N.F. Jr, Madrid M.Y., Langer R., J. Appl. Polym. Sci., **46** (1992) 19
19. Higuchi T., J. Pharm. Sci., **50** (1961) 874
20. Higuchi T., J. Pharm. Sci., **52** (1963) 1145
21. Grass IV G.M., Robinson J.R., in Modern Pharmaceutic II Ed., Banker G.S., Rhodes C.T., Gwen M., Antzen J., Robinson J.R., Marcel Dekker, New York, 1990, 635
22. Flynn G.L., Yalkowsky S.H., Roseman T.J., J. Pharm. Sci., **63** (1974) 479

23. Rhine W.D., Hsieh D.S.T., Langer R., J. Pharm. Sci., **69** (1980) 265
24. Grathwohl P., Diffusion in Natural Porous Media, Kluwer Academic Publ., London, (1998)
25. Sahimi M., Application of Percolation Theory, Taylor & Francis, London, (1994)
26. Caraballo I., Millàn M., Fini A., Rodriguez L., Cavallari C., J. Controlled Release, **69** (2000) 345
27. Hilyard N.C., Cunningham A., Low Density Cellular Plastics, Chapman & Hall, (1994), London
28. Hilyard N.C., Mechanics of Cellular Plastic, Applied Science Publishers Ltd, (1982), London
29. Gibson L.J., Ashby M.F., Cellular Solids, Structure and Properties, Pergamon Press, Oxford, (1988)
30. Roberts A.P., Garboczi E.J., Acta Mater., **49** (2001) 189